

## **Boundary Plasma Characteristics in NSTX Discharges**

R. Maingi, H. W. Kugel, C. J. Lasnier, A. L. Roquemore, V. A. Soukhanovskii, C.E. Bush, and the NSTX Team

### **Abstract**

We report the first results of heat flux scaling experiments in NSTX. We find that the peak heat flux observed in the outer divertor was  $\sim 6 \text{ MW/m}^2$  at 5 MW heating power in lower-single null diverted configuration. The peak heat flux(profile width) was observed to increase(decrease) with heating power. The peak heat flux is lower than predicted by early 2-D edge transport conservative design calculations. However, the total power flow to the divertor is only 15-30% of the input power, suggesting other processes reduce the available open field line power which can be conducted and convected to the target.

### **Introduction**

Spherical Tori (ST) are designed to be compact devices, capable in some designs of reaching higher power density than conventional aspect ratio tokamaks. Existing ST have achieved [1,2] higher (ratio of plasma pressure to vacuum toroidal field) than conventional aspect ratio machines, thereby making more efficient usage of the available toroidal field. A by-product of the ST design is the possibility of increased heat flux to first wall surfaces, because the major radius, and hence surface area, over which to spread the power is reduced. This paper presents the results of the first heat flux scaling experiment on NSTX and compares the measured heat flux to design calculations.

The National Spherical Torus Experiment (NSTX) is a low aspect ratio spherical torus ( $R=0.86\text{m}$ ,  $a = 0.67\text{m}$ ,  $I_p < 1.5 \text{ MA}$ ,  $B_t < 0.6 \text{ T}$ ) capable[3] of being operated in single-null, double-null, or center stack limiter configurations. At present, auxiliary heating consists of up to 5 MW neutral beam injected power and up to 6 MW of high-harmonic fast wave radio-frequency heating. Present edge diagnostics include a divertor infrared (IR) camera for divertor heat flux measurements, two CCD cameras for filtered visible light detection in the divertor and center stack regions, an edge reflectometer for density profiles, and a multi-pulse Thomson Scattering system with several points in the edge and scrape-off layer (SOL). New edge diagnostics in the commissioning process in May 2002 include a second IR camera, a set of divertor flush-mount Langmuir probes, a mid-plane edge fast reciprocating probe, a divertor bolometer system, and a divertor visible camera for fast fluctuations.

### **Experiment and Diagnostic Details**

The IR camera used for these experiments was an Indigo ALPHA compact micro-bolometer camera (7-13  $\mu\text{m}$  IR range) with 160 x 128 pixels and a 30 Hz frame rate. The thermal e-folding

time for this camera was measured to be  $\sim 20$ ms. The video data were captured with a video frame-grabber, yielding an 8-bit dynamic range. The camera and 25 deg. field-of-view (FOV) lens was placed in a magnetic shield near the top of the machine, with a view looking across the lower divertor (fig. 1 – dashed lines show FOV). Fig. 2 shows a typical grayscale image with several NSTX tile features marked; the most obvious features were used to obtain the spatial calibration. A vertical cut in the image corresponds to a radial IR emissivity profile, which is converted to temperature using an in-situ calibration method. The temperature is converted to heat flux using the known temperature-dependent thermal conductivity of the ATJ graphite tiles in the NSTX divertor[4] and a 1-D conduction model of heat transport into the tile bulk[5] as used at DIII-D.

Scaling of the peak divertor heat flux with heating power was achieved by changing the number of NB sources at otherwise constant conditions. Each NB source provides  $\sim 1.6$  MW input power when operated at 80 kV, and intermediate powers were obtained by pulse-width modulation with 20 ms on/off periods, i.e. a 50% duty cycle. Due to the  $\sim 20$ ms thermal e-folding time of the IR camera, discharges with a minimum of 100ms flattop in plasma current were used. For this data set,  $I_p=750$  kA,  $B_t=0.45$  T, and the magnetic divertor was formed at 150ms, and the discharges had L-mode confinement and mid-plane profiles. The average inner and outer wall gaps were 7cm and 5cm respectively. The temporal characteristics of a typical discharge from this experiment are shown in fig. 3. Panel 3b shows the total heating power including NB, ohmic and RF power. Note that RF power was added into most of these discharges from 120-160ms to help extend the plasma current flattop. Panel 3c shows that the peak temperature rose by over  $100^\circ\text{C}$  along the outer divertor target during the NBI heating. Panel 3d shows that the peak heat flux was computed at  $\sim 6$  MW/m<sup>2</sup>, with a profile width (full-width, half-max, FWHM)  $\sim 2$  cm, which is at the lower limit of spatial resolution achievable with the present system and analysis technique.

### **Analysis and Discussion**

Heat flux profiles at several different times of the discharge in fig. 3 are shown in fig. 4. The profile peaks on the outboard divertor ( $R > 50$  cm) within 1-2cm of the magnetic outer strike point from EFIT analysis. It is noteworthy that the profile width is much narrower on the outboard side than the inboard side. At the highest heat flux, the total power flowing to the outer target approached 700 kW, i.e. only a small fraction of the 5 MW average heating power for this discharge during the analysis time. Due to a failure of inboard tile thermocouples during the in-situ calibration, the inboard divertor heat flux is known to only within a factor of 2 for this data set. From the available data, however, it can be estimated that a maximum of 300 kW flowed to the inboard target, yielding a maximum total divertor power of 1 MW. With core radiation measured to be  $\sim 10$ -20% of input power, a significant fraction of heating power is unaccounted, which will be discussed below.

Figure 5 shows the dependence of the outboard peak heat flux and profile width on the loss power, which is computed as the heating power minus a core radiation fraction of 20%. It is observed that the peak heat flux generally increased with loss power (fig. 5a), while the profile width decreased with loss power (fig. 5b). Fig. 5c shows that the peak heat flux increased with decreasing profile width (although this plot could as well be plotted as profile width vs. peak heat flux since the dependent variable is not obvious). In conventional aspect ratio tokamaks, the feature of profile width narrowing as peak heat flux increases has been attributed to formation of an electron conduction channel near the strike point, one signature of which is high electron temperature near the target. This picture will be tested in NSTX upon commissioning of the tile Langmuir probes, but it is nonetheless a candidate explanation for the observed behavior.

Figure 6 compares the highest measured peak flux with 2-D edge plasma calculations[6] with the b2.5 code[7] made during the NSTX design phase, with an improved neutral transport model[8]. The calculations assumed cross-field ion and electron thermal transport coefficients  $\kappa_{i,e}$  of  $4 \text{ m}^2/\text{s}$ , and diffusion coefficient of  $1 \text{ m}^2/\text{s}$ . The calculations were intended as a worst case scenario by eliminating divertor impurity radiation. In these cases, the hydrogenic losses totaled  $\sim 10\%$  of loss power. Increasing the divertor radiated power fraction reduced the inboard heat flux quickly, but the outboard heat flux was reduced significantly only when divertor radiated power fraction exceeded 80%. It is evident that the highest measured peak heat flux of  $6 \text{ MW}/\text{m}^2$  falls well below the range of  $10\text{-}25 \text{ MW}/\text{m}^2$ , predicted with the most pessimistic assumptions for NSTX. A linear fit to the outboard divertor simulations (which passes through the origin) is indicated by the dashed line. The solid star symbol shows the measured NSTX peak heat flux, assuming that the experimental SOL loss power was the 1MW sum estimated to both divertors. Note that the star symbol lies nearly on the dashed fit line, suggesting that the cross-field transport and recycling assumptions made in the design calculations crudely represent the conditions in this experiment. The challenge is to determine the mechanisms which prevent power flowing to the divertor legs. At least four mechanisms may be identified: (1) power flow to the center column, (2) fast ion power loss to the RF antenna during NB operation (3) power radiated via impurities near the X-point and divertor, and. (4) power loss to the walls due to charge exchange in the main chamber and/or divertor region. Partial detachment of plasma from the divertor strike point is implicitly included in (3) and (4) above. Commissioning of the second IR camera in NSTX will allow assessment of (1) and (2) directly, and commissioning of the divertor bolometer will allow assessment of (3). Assessment of (4) will be restricted to determination if the plasma is in a partially detached state, which will be accomplished by examining pressure balance along open field lines after commissioning of the divertor Langmuir probes and possibly the edge reciprocating probe.

## **Summary**

We have shown that the outboard peak heat flux increased with heating power, and that the profile width narrowed. The maximum observed peak heat flux was estimated at  $6 \text{ MW/m}^2$  with a profile width of 2 cm. Total power at the divertor was typically between 15-30% of input power minus a core radiated power fraction. Unaccounted power might be going to the center stack, to the RF antenna as fast ion loss, to the wall as charge exchange neutrals, or might be radiated in the divertor near the X-point. The addition recent diagnostics will allow measurement of several of these loss channels.

For the estimated power flow through the edge, the measured peak heat flux is less than predicted during the NSTX design phase with 2-D edge plasma transport calculations which neglected impurity radiation. However, the measured peak heat flux lies on a linear scaling (vs. loss power) with the 2-D calculations if it is assumed that the experiment loss power equals the power measured at the divertor target. This consistency suggests that the transport coefficients and recycling assumptions made during the design calculations are globally indicative of the L-mode transport observed in the experiment. The next step in this study is to conclusively identify the additional loss mechanisms preventing power from flowing to the divertor.

## **Acknowledgements**

This work is supported by the U.S. Dept. of Energy under contracts DE-AC05-00OR22725, DE-AC02-76CH03073, and W-7405-ENG-36.

## **Figure Captions**

1. NSTX cross-section, showing approximate IR camera field-of-view with dashed arrows.
2. Sample IR camera image. Darker regions indicate higher emissivity and surface temperature.
3. Discharge characteristics of NSTX high NBI power discharge. The working gas in these discharges was either helium or deuterium, and the NB sources were operated in deuterium.
4. Heat flux profiles across the divertor at several different times of discharge. The heat flux profile from the outer divertor for  $R > 50 \text{ cm}$  is known to within  $\sim 20\%$ , whereas the magnitude of the profile inside of 50 cm is known to only within a factor of two due to a calibration difficulty with this dataset.
5. (a) Dependence of peak heat flux on loss power through edge, (b) dependence of profile width (Full-width, half-max) on loss power, and (c) dependence of peak heat flux on profile width. The highest heat fluxes occur at smallest profile widths.
6. Measured peak heat flux vs. design calculations with the b2.5 2-D edge transport code. The loss power for the measured heat flux is estimated as the total power into the outer and inner divertor legs. The dashed line through the origin is a linear fit to the outboard peak heat flux data, and the NSTX datum lies close to the line.

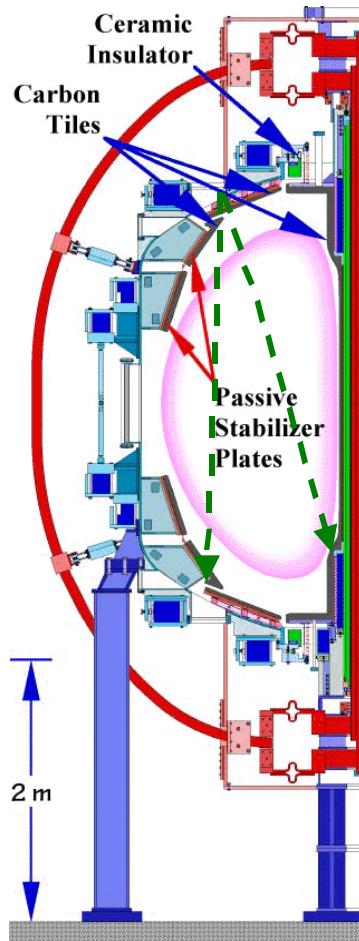


Fig. 1 - NSTX cross-section, showing approximate IR camera field-of-view with dashed arrows.

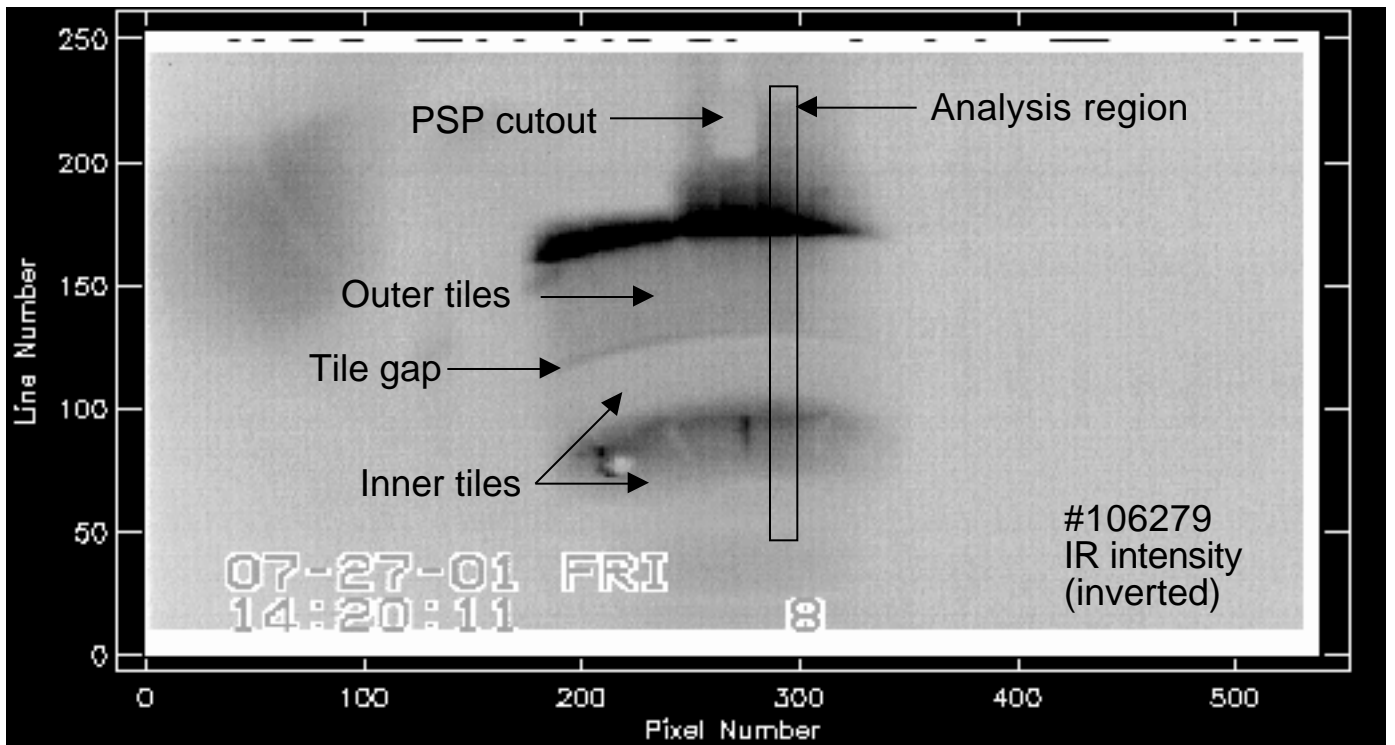


Fig. 2 - Sample IR camera image. Darker regions indicate higher emissivity and surface temperature.

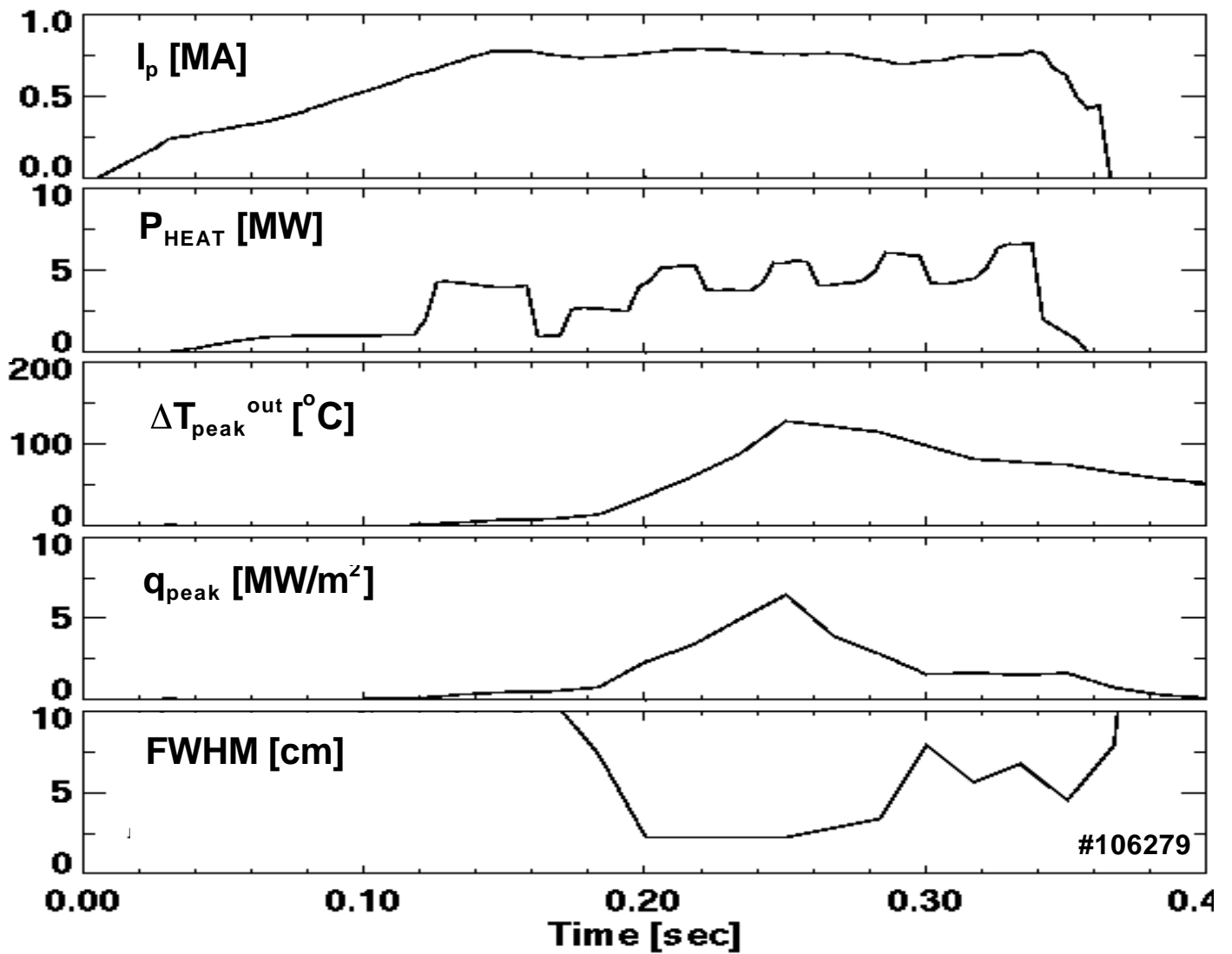


Fig. 3 - Discharge characteristics of NSTX high NBI power discharge. The working gas in these discharges was either helium or deuterium, and the NB sources were operated in deuterium.

Camera 1601 Pass 0 Shot 106279 Pol. Cut Line #11 Time 200 mS

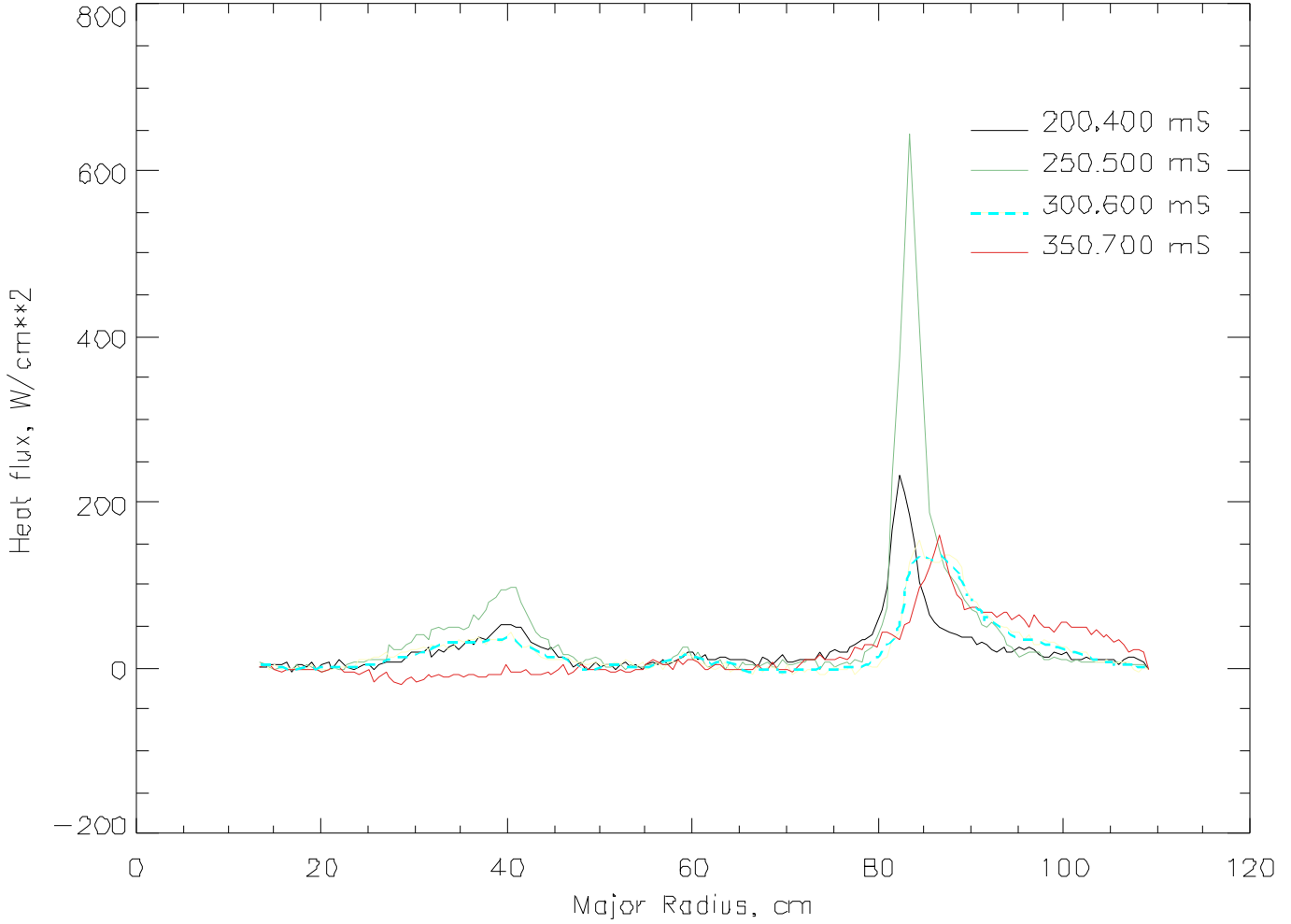


Fig. 4 - Heat flux profiles across the divertor at several different times of discharge. The heat flux profile from the outer divertor for  $R > 50$  cm is known to within  $\sim 20\%$ , whereas the magnitude of the profile inside of 50 cm is known to only within a factor of two due to a calibration difficulty with this dataset.

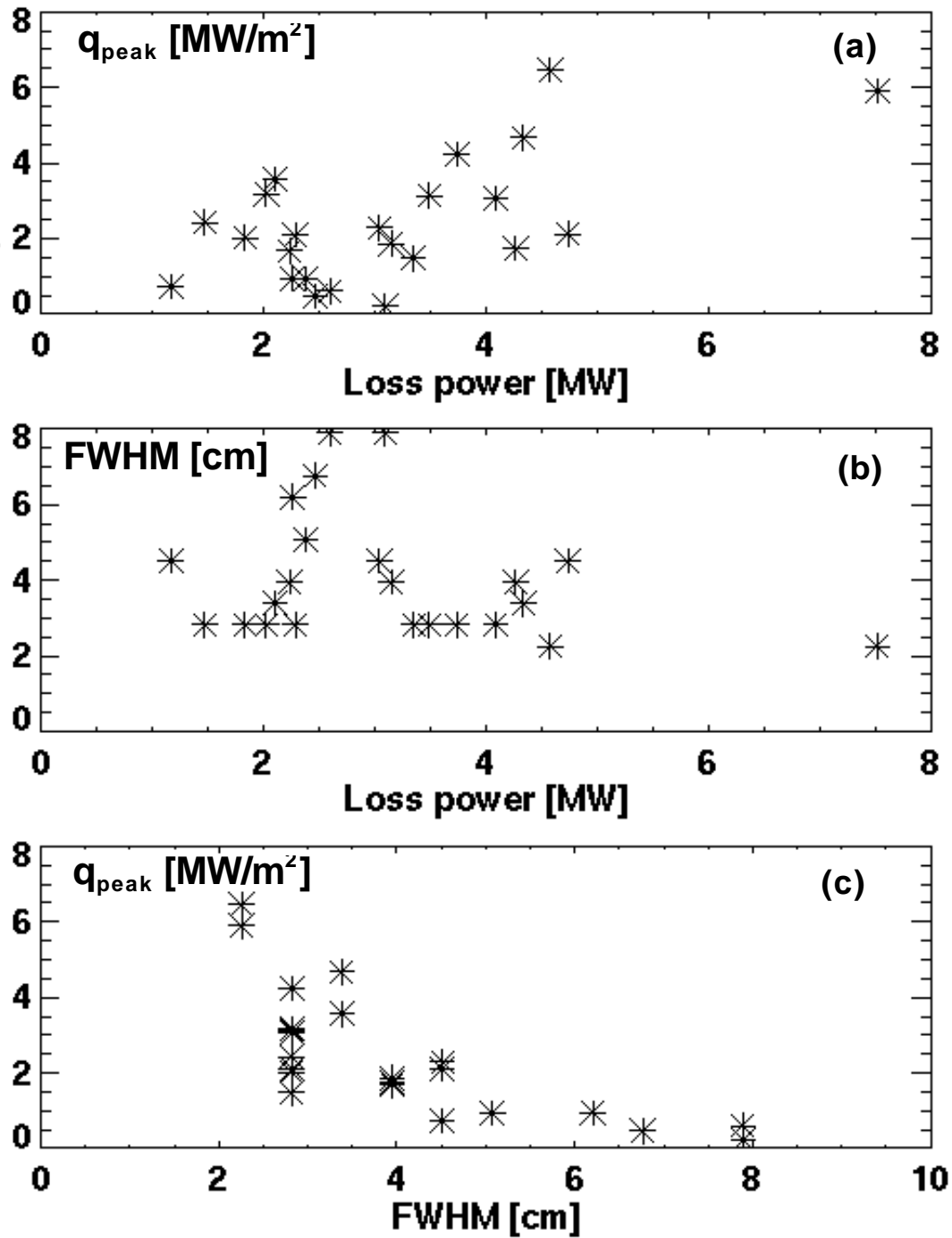


Fig. 5 - (a) Dependence of peak heat flux on loss power through edge, (b) dependence of profile width (Full-width, half-max) on loss power, and (c) dependence of peak heat flux on profile width. The highest heat fluxes occur at smallest profile widths.

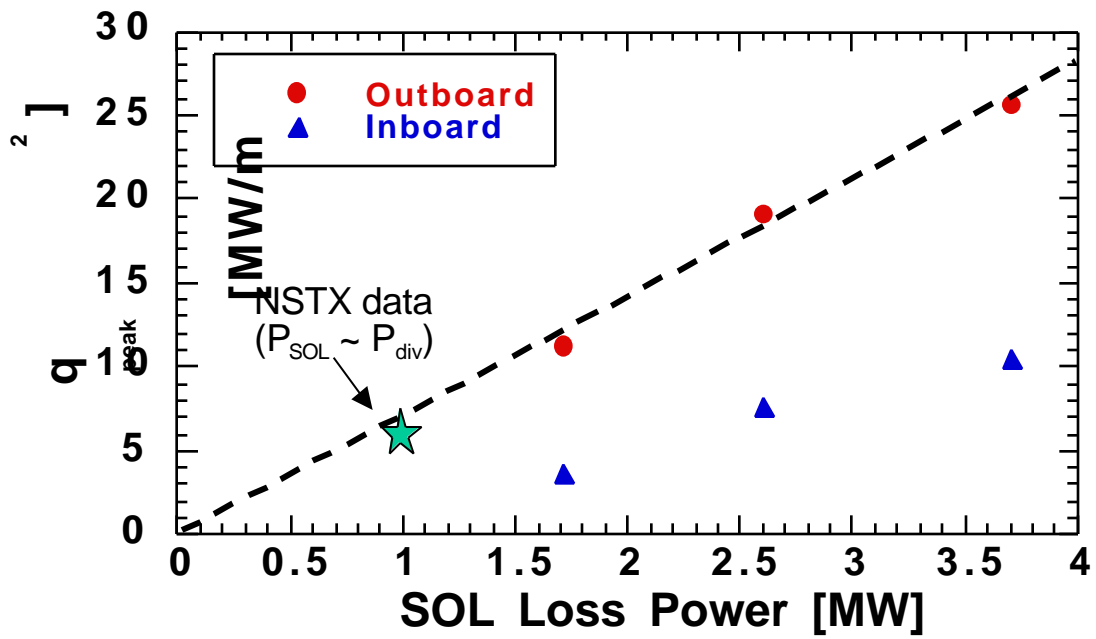


Fig. 6 - Measured peak heat flux vs. design calculations with the b2.5 2-D edge transport code. The loss power for the measured heat flux is estimated as the total power into the outer and inner divertor legs. The dashed line through the origin is a linear fit to the outboard peak heat flux data, and the NSTX datum lies close to the line.

## **References**

---

- <sup>1</sup> D.A. Gates, et. al., *Phys. Plasma* **5** (1998) 1775; M. Graznevich, et. al. *Phys. Rev. Letts.* **80** (4 May 1998) 3972.
- <sup>2</sup> S.A. Sabbagh, et. al., *Phys. Plasma* **9** (2002) 2085.
- <sup>3</sup> M. Ono, et. al., *Nucl. Fusion* **40** (2000) 557.
- <sup>4</sup> H.W. Kugel, et. al., *J. Nucl. Mater.* **290-293** (2001) 1185.
- <sup>5</sup> D.N. Hill, et al., *Rev Sci Instrum.* **61** (1990) 3528; C.J. Lasnier, et al., *Nucl. Fusion* **38** (1998) 1225.
- <sup>6</sup> R. Maingi, et. al., Proc. 1997 International Workshop on Spherical Torus, Sept. 3-5, 1997, St. Petersburg, Russia.
- <sup>7</sup> B.J. Braams, *Contr. Plasma Phys.* **36** (1996) 276.
- <sup>8</sup> R. Maingi, et. al., *Nucl. Fusion* **34** (1994) 283.